Chemical Geology 645 (2024) 121880

Contents lists available at ScienceDirect

Chemical Geology

journal homepage: www.elsevier.com/locate/chemgeo

Positive Δ^{199}Hg anomalies in Mesozoic porphyry Mo deposits of Northeastern China and their implications to the metallogeny of arc-related hydrothermal systems at convergent margins

Lingjian Gao [a,b], Deyou Sun [b], Zhendong Tian [a], Anbo Luo [a], Bernd Lehmann [c], Runsheng Yin [a,*]

[a] State Key Laboratory of Ore Deposit Geochemistry, Institute of Geochemistry, Chinese Academy of Sciences, Guiyang 550081, China
[b] College of Earth Sciences, Jilin University, Changchun 130061, China
[c] Mineral Resources, Technical University of Clausthal, Clausthal-Zellerfeld 38678, Germany

ARTICLE INFO

Editor: Marco Fiorentini

Keywords:
Mercury isotopes
Oceanic plate subduction
Mesozoic epithermal Au—Ag deposits
Porphyry Mo deposits

ABSTRACT

Mercury (Hg) isotopes display unique mass-independent isotope fractionation (MIF, reported as Δ^{199}Hg), which is primarily generated via Hg photochemical processes in the land-ocean-atmosphere system. Magmatic and hydrothermal processes do not trigger MIF of Hg isotopes, therefore, Hg-MIF signals detected in deep reservoirs (mantle and crust) are theoretically sourced from recycled surface materials. Here, we observed positive Δ^{199}Hg signals (0.10 ± 0.07‰, SD) in Mesozoic porphyry Mo deposits of NE China. These values correspond to the recently reported Δ^{199}Hg signature of Mesozoic epithermal Au—Ag systems in NE China (Δ^{199}Hg: 0.11 ± 0.07‰, SD), suggesting that both mineral systems receive large amounts of Hg from subducted marine materials, given that marine Hg has positive Δ^{199}Hg composition. Our study thus provides novel geochemical evidence on the linkage between oceanic plate subduction and metallogeny of various hydrothermal systems at convergent margins. Subduction contributes large amounts of volatiles to arc magmas, which then release metal-rich magmatic-hydrothermal fluids of the porphyry to epithermal ore deposit spectrum.

1. Introduction

Mercury (Hg) is a highly volatile metal of interest not only to environmental chemists due to its potent biotoxicity in humans and ecosystem health, but also to economic geologists due to its close association with a series of metals (e.g., Au, Sb, Pb, Zn) in hydrothermal systems. Decades of research have been dedicated to understanding the Hg biogeochemical cycle in surface environments, while the deep Hg cycle in interior reservoirs remains poorly studied. The available results suggest that Hg is of low abundance in igneous rocks (e.g., basalts and granites), ranging from 0.1 to 10 ppb (Canil et al., 2015; Deng et al., 2022a; Yin et al., 2022; Tian et al., 2023), but with up to 10^2–10^4 ppb in shallow hydrothermal systems (Xu et al., 2018; Fu et al., 2020; Deng et al., 2021, 2022b). The depletion of Hg in igneous rocks has been attributed to magma degassing of volatile Hg(0) (Zambardi et al., 2009). Plate tectonics is potentially a key driving force for the generation of Hg-bearing hydrothermal deposits (e.g., epithermal Hg-Au-Ag deposits and porphyry Cu—Mo deposits), as they are concentrated in two mainly mercuriferous belts (the Circum Pacific belt and the Mediterranean-Himalayan belt) that cover convergent plate boundaries (Fig. 1A) (Gustin et al., 1999; Rytuba, 2003). Yet, our understanding of the geochemical fate of Hg during hydrothermal processes remains incomplete, and a knowledge gap still exists regarding the linkage between plate subduction and Hg enrichment in arc-related hydrothermal systems.

Mercury isotopes offer a useful tool to address the above-mentioned questions. The seven natural stable isotopes of Hg (196, 198–202, 204 amu) undergo both mass-dependent fractionation (MDF, defined as δ^{202}Hg) and mass-independent fractionation (MIF, typically expressed as Δ^{199}Hg) (Bergquist and Blum, 2007). While a variety of physical, chemical, and biological processes can trigger Hg-MDF, Hg-MIF mainly occurs during photochemical reactions with little interference from other processes (Blum et al., 2014). Hg(II) photoreduction in the surface environment results in mainly negative Δ^{199}Hg values in terrestrial systems (e.g., soil and vegetation) and mainly positive Δ^{199}Hg values in marine systems (e.g., seawater and marine sediments) (Blum et al., 2014), while the primitive mantle displays near-zero Δ^{199}Hg of 0.0 ± 0.1‰ (2SD) (Moynier et al., 2021). The distinctive Δ^{199}Hg values

* Corresponding author.
E-mail address: yinrunsheng@mail.gyig.ac.cn (R. Yin).

https://doi.org/10.1016/j.chemgeo.2023.121880
Received 8 July 2023; Received in revised form 3 December 2023; Accepted 6 December 2023
Available online 12 December 2023

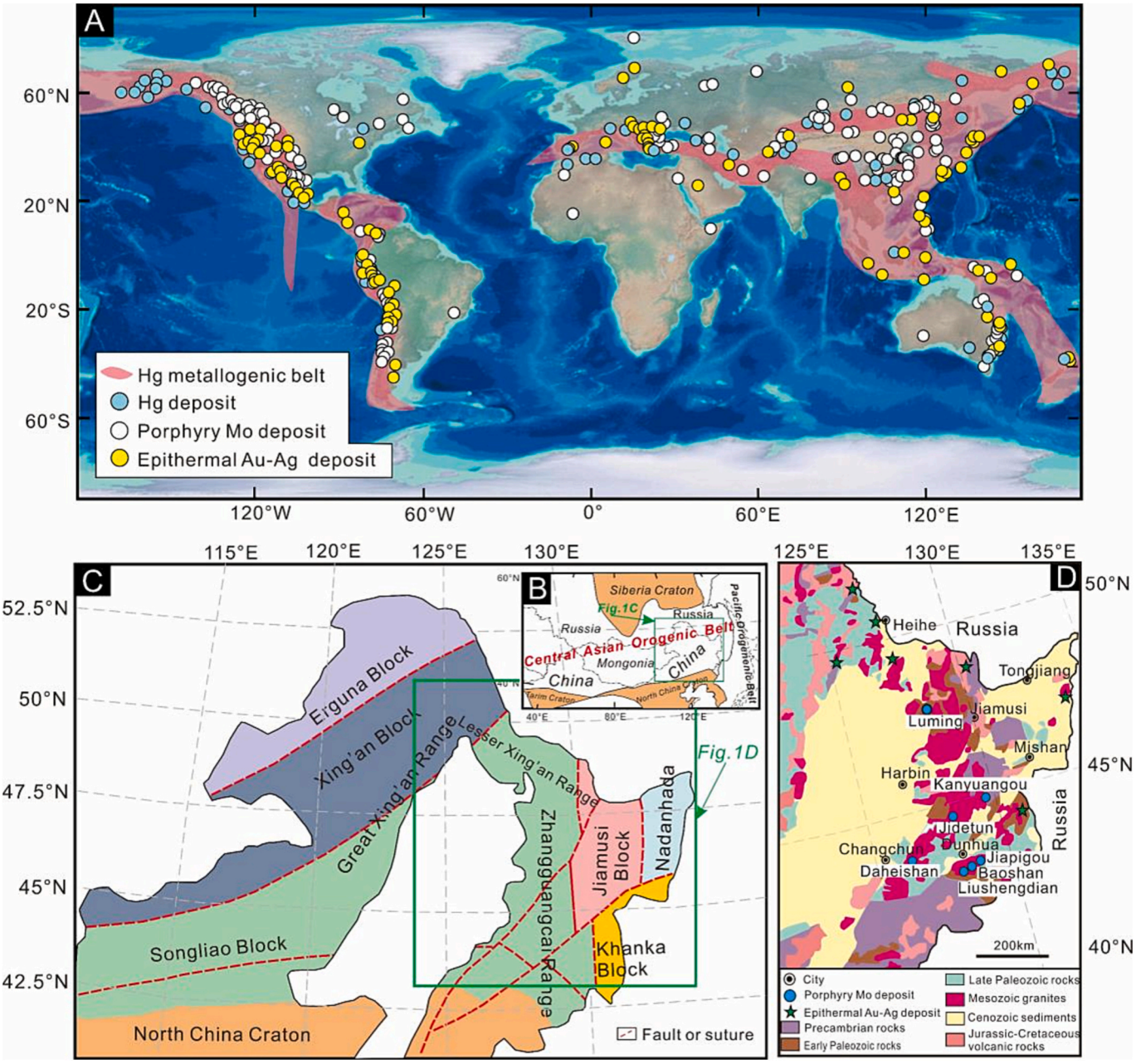

Fig. 1. Maps showing (A) global distribution of major Hg deposits after Rytuba (2003), Mo deposits after Huang et al. (2015) and epithermal Au—Ag deposits after Wang et al. (2019), (B) regional geotectonic setting of Northeast China after Safonova and Santosh (2014), (C) tectonic subdivisions of Northeast China after Xu et al. (2013) and (D) geological map of the eastern part of Jilin and Heilongjiang provinces and the location of porphyry Mo deposits after Chen et al. (2017) and Hou et al. (2017b) and epithermal Au—Ag deposits after Deng et al. (2021).

between crustal and mantle reservoirs suggest that Δ^{199}Hg is diagnostic of surface Hg recycling into deep reservoirs. For instance, recent studies demonstrated positive Δ^{199}Hg values (0 to 0.4‰) in arc-related epithermal Au—Ag deposits and igneous rocks, suggesting that Hg was sourced from recycled marine materials via oceanic plate subduction (Deng et al., 2021, 2022a; Yin et al., 2022). Intracontinental epithermal Pb-Zn-Au-Sb deposits in the South China Craton show negative Δ^{199}Hg values (−0.4 to 0‰), suggesting that Hg derived from terrestrial basement rocks via intracrustal fluid circulation (Xu et al., 2018; Fu et al., 2020; Deng et al., 2022b). The Hg isotopic composition of high-temperature hydrothermal systems (e.g., porphyry deposits) is so far not studied, however.

Abundant middle- to late-Mesozoic epithermal Au—Ag deposits and porphyry deposits (Supplementary Table S1) are distributed in NE China, which is a part of the Circum Pacific mercuriferous belt (Fig. 1). The metallogeny of these deposits is spatially and temporally correlated with subudution of the Paleo-Pacific Ocean plate (Ouyang et al., 2013; Chen et al., 2017). Thus, investigation of Hg isotope in these deposits offers a window to study the deep Hg cycle, in particular, assessing the role of plate subduction on the formation of Hg-bearing hydrothermal systems. The Hg abundance and isotopic composition of Mesozoic igneous rocks and epithermal Au—Ag deposits in NE China have been recently investigated (Deng et al., 2021, 2022a). Here, we extend the work to Mesozoic porphyry Mo deposits in NE China (Fig. 1B). By comparing our new results with previous data on Mesozoic igneous rocks and epithermal Au—Ag deposits in NE China, this study aims to gain a comprehensive understanding of the sources and fates of Hg in hydrothermal systems, and their metallogeny of convergent margins.

2. Geological setting

2.1. Regional geology

NE China is situated between the Siberia and North China cratons and belongs to the eastern segment of the Paleozoic to Mesozoic Central Asian orogenic belt and the Mesozoic-Cenozoic Circum-Pacific orogenic belt (Fig. 1B). The eastern part of Jilin and Heilongjiang provinces (EJHP), located in the eastern segment of NE China, is bounded by the Bureya Massif to the north, the Sikhote-Alin accretionary complex belt to the east, and the Xing'an Terrane to the west (Fig. 1C). The basement of this region consists of Precambrian rocks (gneiss, amphibolite, marble, and tonalite-trondhjemite-granodiorite rocks). The overlying strata consist of carbonate rocks, volcaniclastic rocks, detrital sediments (sandstone, silt sandstone) and metamorphic rocks (marble, slate) of Paleozoic to Cenozoic age (Chen et al., 2017; Li et al., 2023). Granitic magmatism of the Paleozoic and dominantly Mesozoic age is widespread. Following the end-Triassic closure of the Paleo-Asian Ocean, magmatism in NE China was dominated by subduction of the Paleo-Pacific Ocean plate (Li et al., 2023), with abundant Mesozoic volcanic rocks and associated epithermal Au—Ag deposits and porphyry Mo deposits (Ouyang et al., 2013; Chen et al., 2017). The geological background of Mesozoic igneous rocks and epithermal Au—Ag deposits have been described previously (Deng et al., 2021, 2022a).

Mesozoic porphyry Mo deposits in EJHP are genetically associated with granitic batholiths (granodiorite, granodiorite porphyry, monzogranite, monzogranite porphyry, granite porphyry and quartz diorite) (Chen et al., 2017). They are predominately distributed in the Lesser Xing'an Range (LXR) and the mid-eastern Jilin Province (MJP) (Fig. 1D). The LXR is situated in the northern part of the EJHP, and known porphyry Mo deposits in this region are Huojihe, Luming, Cuiling, Ganggangshan and Kanchuangou deposits (Chen et al., 2017). The MJP is situated in the southern part of EJHP, and known porphyry Mo deposits include Fuanpu, Jidetun, Daheishan, Xingshan, Dashihe, Liushengdian, Baoshan, Houdaomu, and Jiapigou deposits in this area (Chen et al., 2017; Hou et al., 2017a).

In this paper, seven porphyry Mo deposits in the EJHP (Luming, Kanchuangou Jidetun, Daheishan, Jiapigou, Liushengdian, and Baoshan deposits) were chosen for study (Fig. 1D). Based on LA-ICP-MS U—Pb dating of granites and *Re*—Os isochron dating of molybdenite, the diagenesis and metallogenesis of these deposits in the EJHP can be divided into three stages: 1) Early Jurassic including the ~180 Ma Luming deposit (Ouyang et al., 2021), one of the largest Mo deposits in NE China, and the ~188 Ma Jiapigou deposit (Wang et al., 2013); 2) Middle Jurassic including the ~170 Ma Jidetun deposit (Zhang et al., 2013), the ~170 Ma Daheishan deposit (Zhou et al., 2014), the ~170 Ma Liushengdian deposit (Wang et al., 2011) and the ~165 Ma Baoshan deposit (Hou et al., 2017a); and 3) late Early Cretaceous including the ~111 Ma Kanchuangou deposit (Hou et al., 2017a). Metallogenic age and geochemical data suggested the formation of these deposits are a consequence of the subduction of the Paleo-Pacific plate (Ouyang et al., 2013; Hou et al., 2017a; Ouyang et al., 2021). The geological features of the porphyry Mo-bearing granitoids studied have been described previously (Hou et al., 2017a; Hou et al., 2017b).

2.2. Deposit geology

The giant Luming porphyry Mo deposit with reserve of 0.75 Mt. Mo at an average grade of 0.092 wt% is in magmatic belt of the Lesser Xing'an Range in Heilongjiang Province. The orebodies are hosted in NW trending altered fault zones in the Mesozoic granitoids. The mineralization at Luming, as a consequence of multiple pulsed release of ore-forming magmas and fluids (Ouyang et al., 2021), mainly occurs as veinlet, stockwork vein, disseminated and brecciated sulfides in monzogranite, granite porphyry and syenogranite suites. Major metal sulfide minerals consist of molybdenite and pyrite, and minor chalcopyrite, hematite, magnetite and pyrrhotite are present. The gangue minerals mainly consist of quartz, feldspar, and biotite, followed by minor illite, kaolin, chlorite, and calcite. The wall rock alteration includes K-feldspathization, silicification, sericitization, chloritization and propylitization, but the mineralization is mainly related to K-feldspathization and silicification. Fluid inclusion studies indicate that the ore-forming fluids belong to the H_2O-NaCl-CH_4 (CO_2) system, with moderate-high salinity (1.6% to 53.1% $NaCl_{eqv}$) and high temperatures (334 °C to 437 °C) (Wang et al., 2015). Recent study proposed partial melting of the juvenile lower crust inherited abundant subducted oceanic sediments with Mo caused metallogenies of Luming deposit (Qu et al., 2022).

The Kanchuangou Mo deposit with an average grade of 0.225 wt% Mo (Hou et al., 2017a), is located in Muling County in Heilongjiang Province, in the southeastern part of the Jiamusi Block. The granodiorite-hosted orebodies with veinlet, stockwork vein, and disseminated sulfides are hosted in Heilongjiang Formation. Metal sulfide minerals at Kanchuangou consist of molybdenite, pyrite, chalcopyrite, and magnetite. The gangue minerals mainly consist of quartz, feldspar, and biotite, hornblende, epidote, chlorite, and calcite. Wall rock alteration includes K-feldspathization, silicification, sericitization, kaolinization and carbonatation. The main mineralization occurred in silicified alteration zones. Geochemical data suggested ore formation is associated with the subduction of the Paleo-Pacific plate (Liu et al., 2010).

The Jidetun porphyry Mo deposit contains 35 t Mo at an average grade of 0.106 wt% (Hou et al., 2017a), and is located in Sulan County, central Jilin Province. The Mo mineralization is generally hosted by monzogranite and quartz diorite intrusions and the orebodies contain quartz veinlet and disseminated ores. Major metal sulfide minerals consist of molybdenite and pyrite, followed by minor chalcopyrite, galena, magnetite and pyrrhotite. The gangue minerals mainly consist of quartz. Wall rock alteration includes K-feldspathization, silicification, sericitization, kaolinization and carbonatation. The Mo mineralization mainly occurred in K-feldspathization and silicification alteration zones. The initial ore-forming fluids belong to NaCl-H_2O system and have high temperature (347 °C to 397 °C) and high salinity features (42 to 47 wt% $NaCl_{eqv}$), and can be attributed to the tectonic-magmatic hydrothermal event that occurred in the Middle Jurassic due to the subduction of the Paleo-Pacific Plate (Wang et al., 2017).

The Jiapigou Mo deposit with an average grade of 0.095 wt% Mo is a recently discovered porphyry Mo deposit in Wangqing county, Jilin Province (Hou et al., 2017a). The main mineralization is hosted by porphyritic monzogranite and the orebodies contain stockwork vein and disseminated ores. Major metal sulfide minerals consist of molybdenite, followed by minor chalcopyrite and pyrite. The gangue minerals mainly consist of quartz, feldspar, and biotite, chlorite, and calcite. The Mo mineralization mainly occurred in K-feldspathization and silicification alteration zones. The ore-forming materials of the deposit may originate from the thickened lower crust during Paleo-Pacific Plate subduction (Wang et al., 2013).

The recently discovered Baoshan porphyry Mo deposit with 3.9 t Mo at an average grade of 0.054 wt% (Hou et al., 2017a), is located in Au'tu county, Jilin Province. The granitoid-hosted orebodies contain filmy and disseminated mineralization. Metal sulfide minerals consist of molybdenite, pyrite, chalcopyrite, magnetite and pyrrhotite. The gangue minerals mainly consist of quartz, feldspar, biotite. The wall rock alteration contains K-feldspathization, silicification, sericitization, chloritization, carbonatization and propylitization. The metallogeny at Baoshan is associated with Paleo-Pacific Plate subduction (Hou et al., 2017a).

The giant Daheishan porphyry Mo deposit is the largest Mo deposit in NE China, containing 1.09 Mt. Mo with an average Mo grade of 0.07 wt % (Zhang et al., 2015), and located in Yongji county, Jilin Province. The mineralization mainly occurred in granodiorite porphyry to form huge single orebody. The orebody contains veinlet, stockwork vein,

Table 1
THg concentration and Hg isotopic composition of samples collected from Mesozoic porphyry Mo deposits of NE China.

Sample ID	Type	THg	$\delta^{199}Hg$	$\delta^{200}Hg$	$\delta^{201}Hg$	$\delta^{202}Hg$	$\Delta^{199}Hg$	$\Delta^{200}Hg$	$\Delta^{201}Hg$
		ppb	‰	‰	‰	‰	‰	‰	‰
Luming Mo deposit									
LM-1	Ore	7.46	−0.32	−0.68	−1.03	−1.39	0.04	0.02	0.02
LM-2	Granite	3.06	−0.45	−0.87	−1.39	−1.82	0.00	0.04	−0.03
LM-3	Granite	5.17	−0.40	−0.75	−1.14	−1.47	−0.03	−0.01	−0.04
LM-4	Granite	3.17	−0.72	−1.45	−2.20	−2.88	0.01	0.00	−0.04
LM-5	Ore	6.09	−0.09	−0.53	−0.68	−1.07	0.18	0.01	0.13
LM-6	Ore	10.8	−0.27	−0.71	−1.03	−1.43	0.09	0.01	0.04
LM-7	Ore	14.8	−0.20	−0.43	−0.67	−0.88	0.02	0.01	−0.01
LM-8	Molybdenite	18.6	−0.38	−0.92	−1.23	−1.84	0.08	0.00	0.15
LM-9	Ore	6.09	−0.64	−1.48	−2.24	−3.01	0.12	0.03	0.02
LM-10	Molybdenite	18.6	−0.15	−0.49	−0.79	−1.17	0.15	0.09	0.09
LM-11	Ore	15.3	−0.46	−1.11	−1.64	−2.32	0.12	0.06	0.11
LM-12	Molybdenite	26.9	−0.32	−0.72	−0.98	−1.31	0.01	−0.06	0.01
LM-13	Ore	17.2	−0.65	−1.51	−2.20	−2.92	0.09	−0.04	−0.01
LM-14	Molybdenite	27.2	−0.55	−1.26	−1.83	−2.38	0.05	−0.06	−0.04
LM-15	Ore	10.7	−0.30	−0.77	−1.13	−1.57	0.10	0.02	0.06
Jiapigou Mo deposit									
JPG-1	Ore	14.2	−0.38	−0.73	−1.12	−1.50	0.00	0.02	0.01
JPG-2	Molybdenite	45.3	−0.17	−0.56	−0.73	−1.13	0.12	0.01	0.13
JPG-3	Molybdenite	26.5	−0.34	−1.08	−1.51	−2.23	0.23	0.04	0.16
JPG-4	Ore	15.2	−0.05	−0.51	−0.65	−1.15	0.24	0.06	0.21
JPG-5	Molybdenite	66.0	−0.30	−0.83	−1.10	−1.57	0.09	−0.04	0.09
JPG-6	Granite	0.71	−0.30	−0.74	−1.10	−1.46	0.07	−0.01	−0.01
JPG-7	Molybdenite	19.9	−0.34	−0.72	−1.08	−1.48	0.03	0.03	0.03
Baoshan Mo deposit									
BS-1	Ore	39.2	−0.23	−0.45	−0.72	−0.97	0.02	0.04	0.02
BS-2	Molybdenite	57.6	−0.18	−0.32	−0.75	−0.91	0.05	0.14	−0.07
BS-3	Ore	53.4	−0.46	−0.91	−1.38	−1.85	0.01	0.02	0.02
BS-4	Ore	8.22	−0.11	−0.42	−0.59	−0.78	0.09	−0.02	−0.01
BS-5	Ore	32.8	−0.24	−0.69	−0.97	−1.29	0.09	−0.04	0.00
BS-6	Granite	1.94	−0.37	−0.72	−1.06	−1.35	−0.03	−0.04	−0.04
BS-7	Granite	1.08	−0.18	−0.39	−0.57	−0.77	0.01	0.00	0.00
BS-8	Ore	102	−0.11	−0.51	−0.69	−1.01	0.14	−0.01	0.07
BS-9	Molybdenite	176	−0.18	−0.58	−0.83	−1.16	0.11	0.01	0.05
BS-10	Molybdenite	111	−0.07	−0.62	−0.69	−1.19	0.23	−0.02	0.21
Daheishan Mo deposit									
DH-1	Ore	89.9	−0.04	−0.37	−0.46	−0.74	0.14	0.00	0.10
DH-2	Ore	137	−0.07	−0.48	−0.68	−1.06	0.20	0.06	0.12
DH-3	Ore	13.2	−0.23	−0.65	−0.98	−1.38	0.12	0.05	0.06
DH-4	Ore	32.1	−0.29	−0.69	−0.94	−1.28	0.03	−0.05	0.02
DH-5	Ore	2.18	−0.33	−0.91	−1.37	−1.94	0.16	0.06	0.09
DH-6	Ore	20.0	−0.29	−1.03	−1.37	−2.10	0.24	0.03	0.21
DH-7	Ore	6.10	−0.25	−0.76	−1.12	−1.63	0.16	0.06	0.11
DH-8	Ore	5.22	−0.39	−0.94	−1.38	−1.95	0.11	0.04	0.09
DH-9	Molybdenite	77.6	−0.60	−1.50	−2.19	−3.07	0.17	0.04	0.11
DH-10	Molybdenite	181	−0.52	−1.38	−1.93	−2.71	0.16	−0.02	0.11
DH-11	Molybdenite	34.3	−0.35	−0.79	−1.25	−1.72	0.08	0.07	0.05
DH-12	Ore	5.79	−0.12	−0.48	−0.65	−0.94	0.11	−0.01	0.06
DH-13	Molybdenite	54.1	−0.16	−0.38	−0.56	−0.91	0.07	0.07	0.12
Liushengdian Mo deposit									
LSD-1	Ore	14.1	−0.29	−0.67	−0.94	−1.36	0.06	0.01	0.08
LSD-2	Granite	5.09	−0.22	−0.55	−0.75	−1.10	0.06	0.00	0.07
LSD-3	Molybdenite	54.9	−0.48	−1.15	−1.77	−2.34	0.11	0.03	−0.01
LSD-4	Granite	7.81	−0.22	−0.55	−0.79	−1.08	0.06	−0.01	0.02
LSD-5	Ore	16.5	−0.21	−0.42	−0.69	−0.97	0.03	0.06	0.04
LSD-6	Ore	79.6	−0.23	−0.59	−0.82	−1.17	0.07	0.00	0.06
LSD-7	Ore	21.6	−0.26	−0.40	−0.55	−0.74	−0.07	−0.02	0.01
LSD-8	Ore	43.8	−0.26	−0.84	−1.21	−1.68	0.16	0.00	0.05
LSD-9	Molybdenite	114	−0.49	−1.18	−1.81	−2.38	0.11	0.01	−0.02
Jidetun Mo deposit									
JD-1	Ore	13.3	−0.32	−0.85	−1.27	−1.77	0.13	0.04	0.06
JD-2	Ore	13.1	−0.38	−0.95	−1.33	−1.89	0.09	0.00	0.09
Kanchuangou Mo deposit									

(*continued on next page*)

Table 1 (*continued*)

Sample ID	Type	THg	δ^{199}Hg	δ^{200}Hg	δ^{201}Hg	δ^{202}Hg	Δ^{199}Hg	Δ^{200}Hg	Δ^{201}Hg
		ppb	‰	‰	‰	‰	‰	‰	‰
KC-1	Ore	7.11	−0.55	−1.17	−1.83	−2.42	0.06	0.05	−0.01
KC-2	Granite	2.79	−0.51	−1.11	−1.57	−2.16	0.03	−0.02	0.05
KC-3	Granite	2.00	−0.43	−0.80	−1.23	−1.55	−0.04	−0.02	−0.07
KC-4	Granite	5.10	−0.38	−0.68	−1.02	−1.30	−0.05	−0.02	−0.05
KC-5	Granite	0.52	−0.09	−0.33	−0.50	−0.65	0.08	−0.01	−0.01
KC-6	Molybdenite	86.2	−0.51	−1.23	−1.81	−2.46	0.11	0.01	0.05
KC-7	Molybdenite	84.0	−0.58	−1.40	−2.13	−2.85	0.14	0.03	0.01

brecciated and disseminated ores. Major metal sulfide minerals consist of molybdenite and pyrite, followed by minor chalcopyrite, sphalerite, magnetite and pyrrhotite. The gangue minerals mainly consist of quartz, feldspar, biotite, and chlorite. The initial ore-forming fluids belong to NaCl-H_2O system with high temperature (400 to 500 °C) and high salinity (~21 wt% NaCleqv) (Zhou et al., 2015). Zhou et al. (2018) stated Mo at Daheishan Deposit sourced from the shales overlying the oceanic plate due to subduction of Mudanjiang Ocean driven by the westward subduction of the Paleo-Pacific Ocean.

The Liushengdian Mo deposit with an average Mo grade of 0.075 wt % (Zhang et al., 2015), is located in An'tu county, Jilin Province. The Mo mineralization mainly occurred in monzonitic granite porphyry. The orebodies contain veinlet and disseminated ores. Major metal sulfide minerals consist of molybdenite, followed by minor pyrite, chalcopyrite, sphalerite. The gangue minerals mainly consist of quartz, feldspar, orthoclase, sericite, calcite, and chlorite. The wall rock alteration contains silicification, sericitization, chloritization, carbonatization, but mineralization mainly occurs in quartz-sericitization altered zones. Re content of the molybdenite suggests that the ore-forming materials might have been derived mainly from the crust and constrained by the subduction of the Pacific plate (Wang et al., 2011).

3. Materials and methods

A total of 64 samples, including 12 granite samples, 31 bulk ore samples and 21 molybdenite samples were collected from the seven ore deposits selected. Detailed information (e.g., location and sample type) of the samples is given in Table 1. The samples were first cut to expose fresh surfaces, washed by 18.2 MΩ·cm water, air-dried, powdered, and homogenized, prior to analysis.

Total Hg concentrations were measured using the Lumex R915+ Hg analyzer at the Institute of Geochemistry, Chinese Academy of Sciences (IGCAS), yielding Hg recoveries of 90%–110% (n = 7) for standard reference material GSS-4 (soil) and uncertainty of <10% for sample duplicates. Based on measured Hg concentrations, samples were then preconcentrated by a double-stage tube furnace coupled with 5 mL of 40% reverse aqua regia (HNO_3/HCl = 2/1, v/v; Zerkle et al., 2020). Standard reference material (GSS-4, soil) was prepared in the same way as the samples to ensure Hg recoveries. The preconcentrated solutions were measured for total mercury (THg) concentrations using F732—S cold vapor atomic absorption spectrometry (CVAAS, Huaguang Ltd., China), prior to Hg isotope measurement.

The Hg-preconcentrated solutions were diluted to 1 ng/mL Hg in 10 to 20% (v/v) acids using 18.2 MΩ·cm water and subjected to Hg isotope analysis using Neptune Plus multi-collector inductively coupled plasma mass spectrometry (MC-ICP-MS) at IGCAS followed a previous method (Yin et al., 2016). Hg isotopic composition was reported following the convention recommended by Blum and Bergquist (2007). Hg-MDF is expressed in δ^{202}Hg notation in units of per mil (‰) referenced to the NIST-3133 Hg standard (analyzed before and after each sample):

$$\delta^{202}\mathrm{Hg}(‰) = \left[\left(^{202}\mathrm{Hg}/^{198}\mathrm{Hg}_{\mathrm{sample}}\right)/\left(^{202}\mathrm{Hg}/^{198}\mathrm{Hg}_{\mathrm{standard}}\right) - 1\right] \times 1000 \quad (1)$$

Hg-MIF is reported in Δ notation, which describes the difference between the measured δ^{xxx}Hg and the theoretically predicted δ^{xxx}Hg

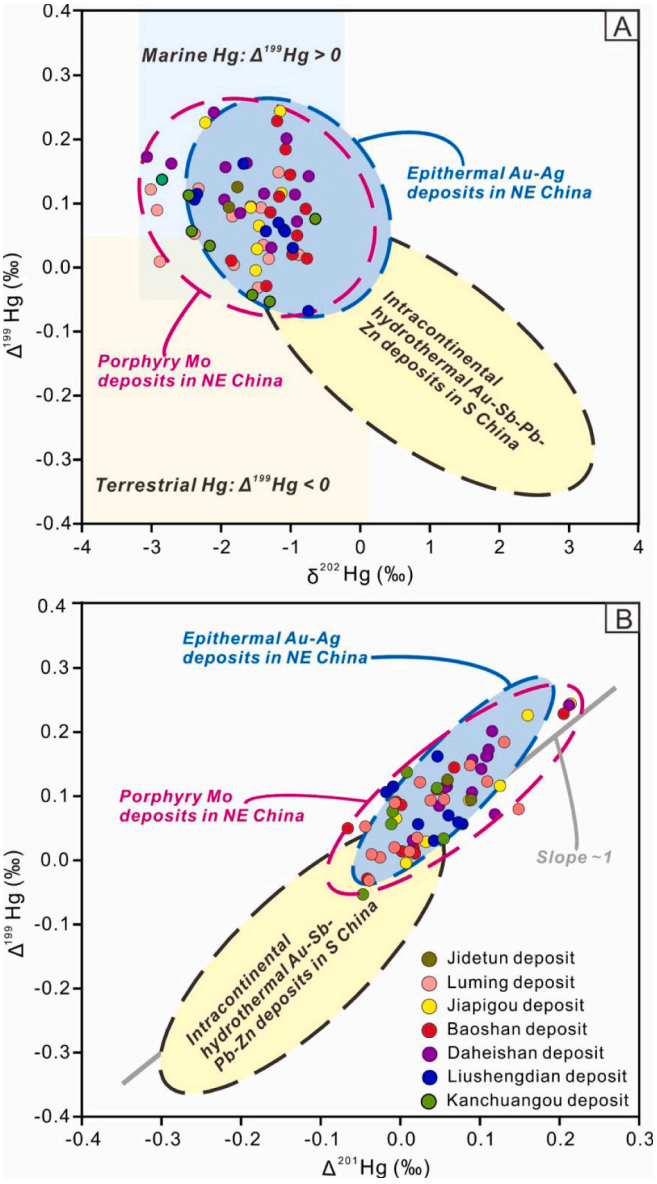

Fig. 2. (A) Δ^{199}Hg versus δ^{202}Hg and (B) Δ^{199}Hg versus Δ^{201}Hg for samples from porphyry Mo deposits in NE China (This study), intracontinental low-temperature Au-Sb-Pb-Zn deposits in South China (Xu et al., 2018; Fu et al., 2020; Deng et al., 2022b) and arc-related epithermal Au—Ag deposits in NE China (Deng et al., 2021). The area of marine sediments is defined by Yin et al. (2015) and Meng et al. (2019), and terrestrial Hg is defined by Blum et al. (2014).

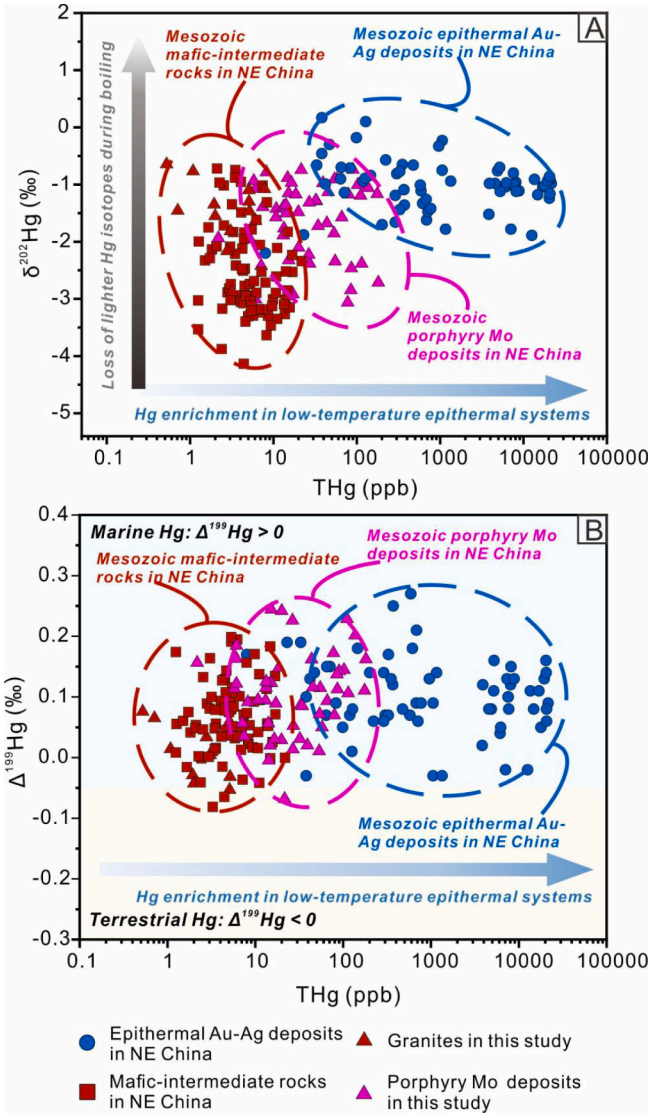

Fig. 3. (A) THg versus δ^{202}Hg and (B) THg versus Δ^{199}Hg for porphyry Mo deposits in NE China (This study), mafic-intermediated rocks in NE China (Deng et al., 2022a) and epithermal Au—Ag deposits in NE China (Deng et al., 2021).

value, in units of per mil (‰):

$$\Delta^{xxx}Hg \approx \delta^{xxx}Hg - \delta^{202}Hg \times \beta \quad (2)$$

β is equal to 0.2520 for ^{199}Hg, 0.5024 for ^{200}Hg and 0.7520 for ^{201}Hg, respectively. Analytical uncertainty was estimated based on the replication of the NIST-3177 secondary standard solutions and GSS-4. NIST-3177 secondary standard solutions and pre-concentrated GSS-4 solutions, diluted to 1 ng/mL Hg in 10% HCl (v/v), were measured in every 10 samples. The overall average and uncertainty of NIST-3177 (δ^{202}Hg: −0.53 ± 0.11‰; Δ^{199}Hg: 0.01 ± 0.05‰; Δ^{200}Hg: 0.02 ± 0.07‰; Δ^{201}Hg: 0.04 ± 0.06‰; 2SD, n = 7) and GSS-4 (δ^{202}Hg: −1.64 ± 0.10‰; Δ^{199}Hg: −0.47 ± 0.03‰; Δ^{200}Hg: −0.02 ± 0.06‰; Δ^{201}Hg: −0.40 ± 0.05‰; 2SD, n = 7) agree well with previous results (Bergquist and Blum, 2007; Zerkle et al., 2020; Deng et al., 2021). The analytical uncertainty of the Hg isotope in this study was reported as 2SD of the samples, and the largest values of standard deviation (2SD) for NIST-3177 and GSS-4 were used to reflect analytical uncertainties.

4. Results

The analytical results are detailed shown in Table 1. Briefly, Hg concentrations vary largely among granite (0.52 to 7.81 ppb, mean 3.0 ± 2.2 ppb, SD), bulk ore (2.18 to 136 ppb, mean 27 ± 32 ppb, SD) and molybdenite samples (18 to 181 ppb, mean 67 ± 49 ppb, SD). All samples show an overall variation of −3.07 to −0.65‰ for δ^{202}Hg and −0.06 to 0.24‰ for Δ^{199}Hg (Fig. 2). No clear differences in δ^{202}Hg were observed among granite (mean − 1.46 ± 0.61‰, SD), bulk ore (mean − 1.50 ± 0.59‰, SD) and molybdenite samples (mean − 1.83 ± 0.07‰, SD). Bulk ore and molybdenite samples show positive Δ^{199}Hg values of 0.10 ± 0.07‰ (SD) and 0.11 ± 0.06‰ (SD), respectively, slightly higher than that for granite samples (0.01 ± 0.05‰, SD) (Fig. 3).

The study of Mesozoic igneous rocks and epithermal Au deposits in NE China yielded low Hg concentrations for mafic rocks (mean 6.12 ± 4.86 ppb, SD), intermediate rocks (mean 6.40 ± 4.10 ppb, SD), and felsic rocks (mean 4.31 ± 4.23 ppb, SD), and extremely high Hg concentrations in epithermal Au—Ag deposits (330 to 21,500 ppb) (Deng et al., 2021, 2022a). The granites studied here show Hg concentrations similar to the previously analyzed igneous rocks (Deng et al., 2022a; Tian et al., 2023), whereas the bulk ore and molybdenite samples show Hg concentrations 1 to 4 orders of magnitude lower than epithermal Au deposits (Fig. 3).

The negative δ^{202}Hg values of the samples studied here are within the range of previous results on Mesozoic igneous rocks (−4.13 to 0.77‰) and epithermal Au—Ag deposits in NE China (−2.20 to 0.10‰) (Deng et al., 2021, 2022a). The near-zero Δ^{199}Hg values for the granites studied here are within the range of previous results for felsic rocks (−0.26 to 0.21‰), but lower than that for mafic rocks (mean 0.07 ± 0.06‰, SD) and intermediate rocks (mean 0.06 ± 0.07‰, SD) in NE China (Deng et al., 2022a). Epithermal Au—Ag deposits in NE China show positive Δ^{199}Hg values of 0.11 ± 0.06‰ (SD) (Deng et al., 2021), similar to our results on bulk ore and molybdenite samples from the porphyry Mo deposits (Fig. 3).

5. Discussion

5.1. Enrichment of Hg in hydrothermal systems with decreasing temperature

There is an increase in Hg concentration from magmatic rocks (0.1 to 10 ppb), porphyry Mo deposits (1 to 10^2 ppb), to epithermal deposits (10^2 to 10^4 ppb) in NE China (Fig. 3). The low Hg abundance in igneous rocks can be explained by preferential loss of Hg from magmatic systems via magma degassing (Zambardi et al., 2009), because most Hg compounds are highly volatile at high-temperature conditions (Lopez-Anton et al., 2010). As Hg is chalcophile, a substantial amount of the Hg released from the magma tend to inter hydrothermal fluids and be incorporated into Hg-bearing sulfides in hydrothermal systems (Sherman et al., 2009), which explains the enrichment of Hg in the porphyry Mo deposits and epithermal deposits. The very elevated Hg concentrations in epithermal deposits, compared to porphyry Mo deposits, are related to the hydrothermal solubility of Hg which mainly becomes fixed under low-temperature conditions (Krupp, 1988).

5.2. Mass-dependent fractionation of Hg isotopes in magmatic-hydrothermal systems

It is interesting to note that relatively higher mean δ^{202}Hg values can be observed in porphyry Mo deposits (mean − 1.60 ± 0.94‰, SD, This study) and epithermal gold deposits (mean − 1.04 ± 0.48‰, SD; Deng et al., 2021) than in subduction-related mafic and intermediate rocks in NE China (mean − 2.50 ± 0.80‰, SD; Deng et al., 2022a) in NE China (Fig. 3). Previous studies suggest small or no Hg-MDF during magmatic processes (Sherman et al., 2009; Moynier et al., 2021; Yin et al., 2022). The negative δ^{202}Hg values of subduction-related mafic and intermediate rocks in NE China was suggested to reflect the recycled marine sediments, given that marine sediments have negative δ^{202}Hg values (−3 to 0‰) (Yin et al., 2015; Meng et al., 2019). Previous studies

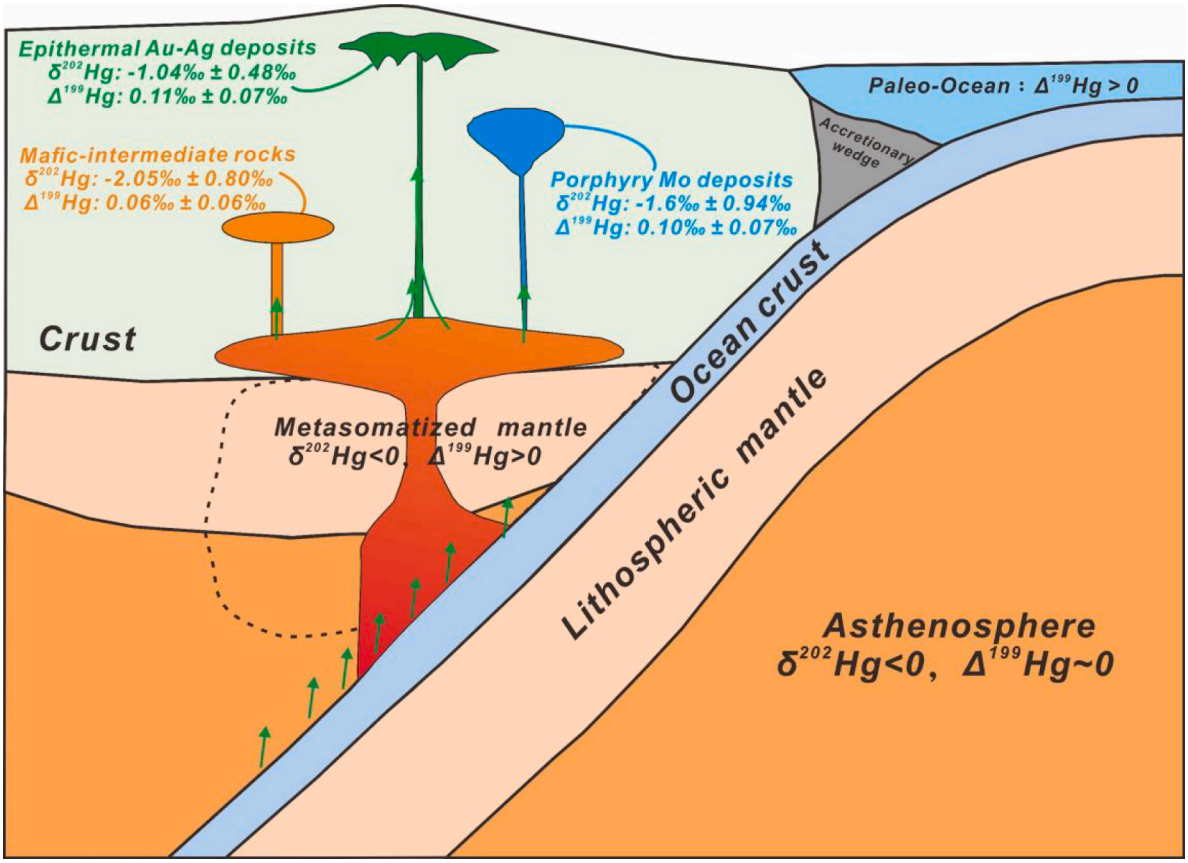

Fig. 4. Schematic model of Hg recycling in arc-related magmatic-hydrothermal systems. The Hg isotopic composition of arc-related epithermal Au deposits, mafic, and intermediate rocks in NE China is based on (Deng et al., 2021, 2022a). The Hg isotopic composition of the asthenosphere is based on Moynier et al. (2021).7

suggested the preferential loss of lighter Hg isotopes from the hydrothermal system via Hg(0) volatilization during hydrothermal fluid boiling (Smith et al., 2005, 2008; Sherman et al., 2009). The increase in mean δ^{202}Hg values from porphyry Mo deposits to epithermal gold deposits in NE China may be explained by the fact that epithermal gold deposits experienced more fluid boiling given the lower temperature and pressure conditions of epithermal systems (Spycher and Reed, 1989; Smith et al., 2005; Scott et al., 2017). However, the large variation of δ^{202}Hg values in ores and the porphyry bulk rocks are complicated to explain currently due to ubiquitous physical and chemical processes generating Hg-MDF (Blum et al., 2014). Instead, we focus Hg-MIF signal as a source tracer, as discussed below.

5.3. Positive Hg-MIF signals indicate marine Hg recycling into porphyry Mo deposits

It is commonly believed that porphyry deposits receive metals mainly from magmatic-hydrothermal fluids (Cooke et al., 2005; Park et al., 2021). Recent studies, based on H-O-S isotopes, suggested that ore-forming materials in Mesozoic porphyry Mo deposits in NE China were essentially derived from magmatic-hydrothermal fluids, whereas the contribution from meteoric water and country rocks can be minor or negligible (Chen et al., 2017; Hou, 2017; Wang et al., 2017; Zeng et al., 2018; Qu et al., 2021). Trace elements (e.g., REE, Sr, Rb, Nb and Re) and metal isotopes (e.g., Hf, Pb, Sr and Nd) in Mesozoic porphyry Mo deposits in NE China further evidence that they have received a substantial amount of recycled metals from subducted marine materials. For instance, Nd—Hf isotopes of Luming deposits (εHf(t): 0.1 to 6.9; εNd(t): −1.84 to −1.37) and Sr-Nd-Pb isotopes of Daheishan deposit (^{87}Sr/^{86}Sr: 0.705413 to 0.707889, εNd(t):-1.28 to +0.92, and ^{206}Pb/^{204}Pb: 18.44 to 18.73) support the presence of subducted oceanic components (Zhou et al., 2018; Qu et al., 2022). Sr-Nd-Pb isotopes of ore-forming granites from Jidetun and Jiapigou deposits (^{87}Sr/^{86}Sr: 0.70404 to 0.70554, εNd (t): −0.9 to 2.4, and ^{206}Pb/^{204}Pb: 15.549 to 15.565) also support the involvement of subducted materials (Zhang et al., 2016). These geochemical evidences have led to the hypotheses that (1) abundant Mo was released from subducted oceanic slab to form Mo-rich hydrothermal fluids, given that marine sediments are commonly rich in Mo (Hou et al., 2017a; Hou et al., 2017b; Zhou et al., 2018; Qu et al., 2022), and (2) oceanic plate subduction also triggered melting of the juvenile lower crust, benefiting formation of porphyry Mo deposits at convergent plate margins (Hu et al., 2014; Zhang et al., 2016; Zhou et al., 2018; Qu et al., 2022). However, questions remain on these hypotheses if Mo has a distinct source with the above-mentioned proxies. Given the close association between Hg and Mo in the porphyry Mo deposits studied, Hg isotopes may provide more direct constraints on the sources of Mo.

In the Δ^{199}Hg vs. Δ^{201}Hg diagram (Fig. 2), all samples show positive Δ^{199}Hg values, with an identical Δ^{199}Hg/Δ^{201}Hg ratio (~1.0) to that observed during seawaters and marine sediments (0.00 to 0.40‰, Blum et al., 2014; Yin et al., 2015), implying that a fraction of Hg in the samples was sourced from marine reservoirs. In addition, bulk ore and molybdenite samples studied here show positive Δ^{199}Hg values (mean 0.10 ± 0.07‰, SD) consistent with that of middle-late Mesozoic epithermal gold deposits (mean 0.11 ± 0.07‰, SD; Deng et al., 2021), mafic rocks (mean 0.07 ± 0.06‰, SD) and intermediate rocks (mean 0.06 ± 0.07‰, SD) in NE China (Deng et al., 2022a), suggesting that Hg in these compartments were largely sourced from subducted marine materials, given that their formation was closely related to Paleo-Pacific plate subduction (Xu et al., 2013; Ouyang et al., 2013, 2021). Consistent with our conclusion, mid-Mesozoic granitoids in NE China, which have a close genetic link to the studied porphyry Mo deposits, display arc-like geochemical features, i.e., enrichment in large ion lithophile elements

and light rare earth elements, and depletion in high field strength elements and heavy rare earth elements (Liu et al., 2010; Wang et al., 2013; Hou et al., 2017a; Hou et al., 2017b). Overall, our results on Δ^{199}Hg values strongly evidence that Hg, by analogy to Mo, in the studied porphyry Mo deposits are largely sourced from recycled marine materials. The consistency in metal sources between this and previous studies, as mentioned above, proves that Hg can be a newly developed petrogenetic tracer on metal sources, which deserves to be used in future studies.

Mesozoic magmatic rocks, porphyry Mo deposits and epithermal Au deposits in NE China are related closely to the subduction of the Paleo-Pacific plate (Xu et al., 2013; Ouyang et al., 2013, 2021). Oceanic plate subduction likely delivered large amounts of ocean-derived materials into the mantle, triggering mantle wedge melting and magmatism to form middle to late Mesozoic igneous rocks and epithermal Au deposits in NE China (Deng et al., 2021, 2022a). The observation of positive Δ^{199}Hg values in porphyry Mo deposits adds new evidence for the contribution of recycled marine Hg (and metals) to arc-related magmatic-hydrothermal systems at convergent plate margins. From another point of view, this study demonstrates a framework regarding Hg cycling at convergent margin settings, i.e., Hg in the subducted oceanic slab can be remobilized, migrated, and involved in mineralization during plate subduction, which may be a main cause of the formation of abundant Hg-bearing hydrothermal systems at the convergent plate boundaries.

6. Conclusions and implications

We observed positive Δ^{199}Hg values for Mesozoic porphyry Mo deposits from NE China, consistent with previous results on Mesozoic epithermal Au systems in this area (Deng et al., 2021). The data suggest that the two hydrothermal systems share a similar Hg or metal source from recycled marine materials due to Hg existing mainly as a solid solution in sulfides (Rytuba, 2003; Deng et al., 2022b). Paleo-Pacific oceanic plate subduction, dehydration, arc magmatism, and associated hydrothermal fluid release at shallow levels provide the framework for this large-scale metal cycling (Fig. 4). Our study highlights the critical role of plate tectonics in controlling the metallogeny of both epithermal deposits and porphyry deposits and provides a novel framework of marine Hg recycling via plate subduction at convergent margins.

Supplementary data to this article can be found online at https://doi.org/10.1016/j.chemgeo.2023.121880.

CRediT authorship contribution statement

Lingjian Gao: Formal analysis, Investigation, Conceptualization, Writing – original draft. **Deyou Sun:** Supervision. **Zhendong Tian:** Formal analysis, Investigation. **Anbo Luo:** Supervision, Writing – review & editing. **Bernd Lehmann:** Supervision, Writing – review & editing. **Runsheng Yin:** Conceptualization, Supervision, Writing – review & editing.

Declaration of Competing Interest

The authors declare that they have no known competing financial interestsor personal relationships that could have appeared to influence the work reported in this paper.

Data availability

The data has been included in the manuscript.

Acknowledgments

This work was supported by the Chinese Academy of Sciences through the Hundred Talent Plan. Editor Marco Fiorentini and an anonymous reviewer were specially thanked for their constructive suggestions that have largely improved the quality of our work.

References

Bergquist, B.A., Blum, J.D., 2007. Mass-dependent and -independent fractionation of Hg isotopes by photoreduction in aquatic systems. Science. 318 (5849), 417–420. https://doi.org/10.1126/science.1148050.

Blum, J.D., Sherman, L.S., Johnson, M.W., 2014. Mercury isotopes in Earth and environmental sciences. Annu. Rev. Earth Planet. Sci. 42 (1), 249–269. https://doi.org/10.1146/annurev-earth-050212-124107.

Canil, D., Crockford, P.W., Rossin, R., Telmer, K., 2015. Mercury in some arc crustal rocks and mantle peridotites and relevance to the moderately volatile element budget of the Earth. Chem. Geol. 396, 134–142. https://doi.org/10.1016/j.chemgeo.2014.12.029.

Chen, Y.-J., Zhang, C., Wang, P., Pirajno, F., Li, N., 2017. The Mo deposits of Northeast China: A powerful indicator of tectonic settings and associated evolutionary trends. Ore Geol. Rev. 81, 602–640. https://doi.org/10.1016/j.oregeorev.2016.04.017.

Cooke, D.R., Hollings, P., Walsh, J.L., 2005. Giant porphyry deposits: Characteristics, distribution, and tectonic controls. Econ. Geol. 100 (5), 801–818. https://doi.org/10.2113/100.5.801.

Deng, C., Sun, G., Rong, Y., Sun, R., Sun, D., Lehmann, B., Yin, R., 2021. Recycling of mercury from the atmosphere-ocean system into volcanic-arc-associated epithermal gold systems. Geology. 49 (3), 309–313. https://doi.org/10.1130/G48132.1.

Deng, C., Gou, J., Sun, D., Sun, G., Tian, Z., Lehmann, B., Moynier, F., Yin, R., 2022a. Mercury isotopic composition of igneous rocks from an accretionary orogen: Implications for lithospheric recycling. Geology. 50 (9), 1001–1006. https://doi.org/10.1130/g50131.1.

Deng, C., Lehmann, B., Xiao, T., Tan, Q., Chen, D., Tian, Z., Wang, X., Sun, G., Yin, R., 2022b. Intracontinental and arc-related hydrothermal systems display distinct δ^{202}Hg and Δ^{199}Hg features: Implication for large-scale mercury recycling and isotopic fractionation in different tectonic settings. Earth Planet. Sci. Lett. 593, 117696 https://doi.org/10.1016/j.epsl.2022.117646.

Fu, S.L., Hu, R.Z., Yin, R.S., Yan, J., Mi, X.F., Song, Z.C., Sullivan, N.A., 2020. Mercury and in situ sulfur isotopes as constraints on the metal and sulfur sources for the world's largest Sb deposit at Xikuangshan, southern China. Miner. Deposita 55 (7), 1353–1364. https://doi.org/10.1007/s00126-019-00940-1.

Gustin, M.S., Lindberg, S., Marsik, F., Casimir, A., Ebinghaus, R., Edwards, G., Hubble-Fitzgerald, C., Kemp, R., Kock, H., Leonard, T., London, J., Majewski, M., Montecinos, C., Owens, J., Pilote, M., Poissant, L., Rasmussen, P., Schaedlich, F., Schneeberger, D., Schroeder, W., Sommar, J., Turner, R., Vette, A., Wallschlaeger, D., Xiao, Z., Zhang, H., 1999. Nevada STORMS project: Measurement of mercury emissions from naturally enriched surfaces. J. Geophys. Res. Atmos. 104 (D17), 21831–21844. https://doi.org/10.1029/1999jd900351.

Hou, X., 2017. Mesozoic Metallogenetic Granitoids from Porphyry Mo Deposit in the Eastern Jilin-Heilongjiang Provinces: Petrogenesis and Molybdenum Mineralization. Jilin University, Changchuan, China (179 pp).

Hou, X.-G., Sun, D.-Y., Gou, J., Yang, D.-G., 2017a. The origin of variable-δ^{18}O zircons in Jurassic and cretaceous Mo-bearing granitoids in the eastern Xing-Meng Orogenic Belt, Northeast China. Int Geol Rev. 61 (2), 129–149. https://doi.org/10.1080/00206814.2017.1411840.

Hou, X.-G., Sun, D.-Y., Gou, J., Yang, D.-G., Li, S., 2017b. Geochronology, geochemistry, and zircon Hf isotopes of the Mo-bearing granitoids in the eastern Jilin-Heilongjiang provinces, NE China: Petrogenesis and tectonic implications. Geol. J. 53 (3), 877–898. https://doi.org/10.1002/gj.2932.

Hu, X., Ding, Z., He, M., Yao, S., Zhu, B., Shen, J., Chen, B., 2014. A porphyry-skarn metallogenic system in the Lesser Xing'an Range, NE China: Implications from U-Pb and Re-Os geochronology and Sr-Nd-Hf isotopes of the Luming Mo and Xulaojiugou Pb-Zn deposits. J. Asian Earth Sci. 90, 88–100. https://doi.org/10.1016/j.jseaes.2014.04.020.

Huang, F., Liu, X.X., Wang, D.H., Wang, C.H., 2015. A preliminary review of metallogenic pegularity of molybdenum deposits in China. Acta Geologica Sinica-English Edition. 89 (3), 972–1001. https://doi.org/10.1111/1755-6724.12492.

Krupp, R., 1988. Physicochemical aspects of mercury metallogenesis. Chem. Geol. 69 (3–4), 345–356. https://doi.org/10.1016/0009-2541(88)90045-9.

Li, G.-Y., Zhou, J.-B., Li, L., 2023. The Jiamusi Block: A hinge of the tectonic transition from the Paleo-Asian Ocean to the Paleo-Pacific Ocean regimes. Earth Sci. Rev. 236, 104279 https://doi.org/10.1016/j.earscirev.2022.104279.

Liu, L., Yanchen, Y., Zhaowu, Y., Shijiong, H., 2010. Geological and geochemical characteristics of Kanchuangou Mo-Cu deposit in Muling of Heilongjiang (in Chinese with English abstract). Global Geology. 29 (3), 413–418. https://doi.org/10.3969/j.issn.1004-5589.

Lopez-Anton, M.A., Yuan, Y., Perry, R., Maroto-Valer, M.M., 2010. Analysis of mercury species present during coal combustion by thermal desorption. Fuel. 89 (3), 629–634. https://doi.org/10.1016/j.fuel.2009.08.034.

Meng, M., Sun, R.Y., Liu, H.W., Yu, B., Yin, Y.G., Hu, L.G., Shi, J.B., Jiang, G.B., 2019. An integrated model for input and migration of mercury in Chinese coastal sediments. Environ. Sci. Technol. 53 (5), 2460–2471. https://doi.org/10.1021/acs.est.8b06329.

Moynier, F., Jackson, M.G., Zhang, K., Cai, H.M., Halldorsson, S.A., Pik, R., Day, J.M.D., Chen, J.B., 2021. The mercury isotopic composition of Earth's mantle and the use of mass independently fractionated Hg to test for recycled crust. Geophys. Res. Lett. 48 (17) https://doi.org/10.1029/2021GL094301.

Ouyang, H.G., Mao, J.W., Santosh, M., Zhou, J., Zhou, Z.H., Wu, Y., Hou, L., 2013. Geodynamic setting of Mesozoic magmatism in NE China and surrounding regions:

Perspectives from spatio-temporal distribution patterns of ore deposits. J. Asian Earth Sci. 78, 222–236. https://doi.org/10.1016/j.jseaes.2013.07.011.
Ouyang, H., Mao, J., Hu, R., Caulfield, J., Zhou, Z., 2021. Controls on the metal endowment of porphyry Mo deposits: Insights from the Luming porphyry Mo deposit, Northeastern China. Econ Geol. 116 (7), 1711–1735. https://doi.org/10.5382/econgeo.4850.
Park, J.-W., Campbell, I.H., Chiaradia, M., Hao, H., Lee, C.-T., 2021. Crustal magmatic controls on the formation of porphyry copper deposits. Nature Reviews Earth & Environment. 2 (8), 542–557. https://doi.org/10.1038/s43017-021-00182-8.
Qu, P., Yang, W., Niu, H., Li, N., Wu, D., 2021. Apatite fingerprints on the magmatic-hydrothermal evolution of the Daheishan giant porphyry Mo deposit, NE China. GSA Bulletin. 134 (7–8), 1863–1876. https://doi.org/10.1130/b36093.1.
Qu, P., Niu, H.-C., Weng, Q., Li, N.-B., Zhao, Y., Zhang, H.-J., 2022. Apatite and zircon geochemistry for discriminating ore-forming intrusions in the Luming giant porphyry Mo deposit, Northeastern China. Ore Geol Rev. 143 https://doi.org/10.1016/j.oregeorev.2022.104771.
Rytuba, J.J., 2003. Mercury from mineral deposits and potential environmental impact. Environ. Geol. 43 (3), 326–338. https://doi.org/10.1007/s00254-002-0629-5.
Safonova, I.Y., Santosh, M., 2014. Accretionary complexes in the Asia-Pacific region: Tracing archives of ocean plate stratigraphy and tracking mantle plumes. Gondw. Res. 25 (1), 126–158. https://doi.org/10.1016/j.gr.2012.10.008.
Scott, S., Driesner, T., Weis, P., 2017. Boiling and condensation of saline geothermal fluids above magmatic intrusions. Geophys. Res. Lett. 44 (4), 1696–1805. https://doi.org/10.1002/2016gl071891.
Sherman, L.S., Blum, J.D., Nordstrom, D.K., McCleskey, R.B., Barkay, T., Vetriani, C., 2009. Mercury isotopic composition of hydrothermal systems in the Yellowstone Plateau volcanic field and Guaymas Basin sea-floor rift. Earth Planet. Sci. Lett. 279 (1–2), 86–96. https://doi.org/10.1016/j.epsl.2008.12.032.
Smith, C.N., Kesler, S.E., Klaue, B., Blum, J.D., 2005. Mercury isotope fractionation in fossil hydrothermal systems. Geology. 33 (10), 825–828. https://doi.org/10.1130/g21863.1.
Smith, C.N., Kesler, S.E., Blum, J.D., Rytuba, J.J., 2008. Isotope geochemistry of mercury in source rocks, mineral deposits and spring deposits of the California Coast Ranges, USA. Earth Planet. Sci. Lett. 269 (3–4), 399–407. https://doi.org/10.1016/j.epsl.2008.02.029.
Spycher, N.F., Reed, M.H., 1989. Evolution of a broadlands-type epithermal ore fluid along alternative P-T paths - Implications for the transport and deposition of base, precious, and volatile metals. Econ. Geol. 84 (2), 328–359. https://doi.org/10.2113/gsecongeo.84.2.328.
Tian, Z., Lehmann, B., Deng, C., Luo, A., Zhang, X., Moynier, F., Yin, R., 2023. Mercury abundance and isotopic composition in granitic rocks: Implications for Hg cycling in the upper continental crust. Geochim. Cosmochim. Acta. https://doi.org/10.1016/j.gca.2023.09.019.
Wang, H., Ren, Y., Zhao, H., Ju, N., Qu, W., 2011. Re-Os dating of molybdenite from the Liushengdian molybdenum deposit in Antu area of Jilin Province and its geological significance (in Chinese with English abstract). Acta Geosci. Sin. 32 (6), 707–715. https://doi.org/10.3975/cagsb.2011.06.08.
Wang, H., Ren, Y., Sun, Z., Hao, Y., Li, C., 2013. Metallogenic epoch and tectonic setting of Jiapigou porphyry molybdenum deposit in Wangqing area, Jilin Province (in Chinese with English abstract). Mineral Deposits 32, 489–500. https://doi.org/10.16111/j.0258-7106.2013.03.002.
Wang, L., Sun, F., Xu, J., Wang, K., Wand, L., Qinglin, X., 2015. Ore-forming fluid and evolution of Luming molybdenum deposit, Heilongjiang Province. Acta Petrologica Sinica. 31 (04), 797–990.
Wang, Z.-G., Wang, K.-Y., Wan, D., Konare, Y., Yang, T.-N., Liang, Y.-H., 2017. Metallogenic age and hydrothermal evolution of the Jidetun Mo deposit in Central Jilin Province, Northeast China: evidence from fluid inclusions, isotope systematics, and geochronology. Ore Geol. Rev. 89, 731–751. https://doi.org/10.1016/j.oregeorev.2017.07.014.
Wang, L., Qin, K.Z., Song, G.X., Li, G.M., 2019. A review of intermediate sulfidation epithermal deposits and subclassification. Ore Geol. Rev. 107, 434–456. https://doi.org/10.1016/j.oregeorev.2019.02.023.
Xu, W.-L., Pei, F.-P., Wang, F., Meng, E., Ji, W.-Q., Yang, D.-B., Wang, W., 2013. Spatial-temporal relationships of Mesozoic volcanic rocks in NE China: Constraints on tectonic overprinting and transformations between multiple tectonic regimes. J. Asian Earth Sci. 74, 167–193. https://doi.org/10.1016/j.jseaes.2013.04.003.
Xu, C.X., Yin, R.S., Peng, J.T., Hurley, J.P., Lepak, R.F., Gao, J.F., Feng, X.B., Hu, R.Z., Bi, X.W., 2018. Mercury isotope constraints on the source for sediment-hosted lead-zinc deposits in the Changdu area, southwestern China. Miner. Deposita 53 (3), 339–352. https://doi.org/10.1007/s00126-017-0743-7.
Yin, R.S., Feng, X.B., Chen, B.W., Zhang, J.J., Wang, W.X., Li, X.D., 2015. Identifying the sources and processes of mercury in subtropical estuarine and ocean sediments using Hg isotopic composition. Environ. Sci. Technol. 49 (3), 1347–1355. https://doi.org/10.1021/es504070y.
Yin, R.S., Krabbenhoft, D.P., Bergquist, B.A., Zheng, W., Lepak, R.F., Hurley, J.P., 2016. Effects of mercury and thallium concentrations on high precision determination of mercury isotopic composition by Neptune Plus multiple collector inductively coupled plasma mass spectrometry. J. Anal. At. Spectrom 31 (10), 2060–2068. https://doi.org/10.1039/c6ja00107f.
Yin, R., Chen, D., Pan, X., Deng, C., Chen, L., Song, X., Yu, S., Zhu, C., Wei, X., Xu, Y., Feng, X., Blum, J.D., Lehmann, B., 2022. Mantle Hg isotopic heterogeneity and evidence of oceanic Hg recycling into the mantle. Nat. Commun. 13, 1–7. https://doi.org/10.1038/s41467-022-28577-1.
Zambardi, T., Sonke, J.E., Toutain, J.P., Sortino, F., Shinohara, H., 2009. Mercury emissions and stable isotopic compositions at Vulcano Island (Italy). Earth Planet. Sci. Lett. 277 (1–2), 236–243. https://doi.org/10.1016/j.epsl.2008.10.023.
Zeng, Q., Guo, W., He, H., Zhou, L., Cheng, G., Su, F., Wang, Y., Wang, R., 2018. He, Ar, and S isotopic compositions and origin of giant porphyry Mo deposits in the Lesser Xing'an Range-Zhangguangcai Range metallogenic belt, Northeast China. J. Asian Earth Sci. 165, 228–240. https://doi.org/10.1016/j.jseaes.2018.04.002.
Zerkle, A.L., Yin, R.S., Chen, C.Y., Li, X.D., Izon, G.J., Grasby, S.E., 2020. Anomalous fractionation of mercury isotopes in the late Archean atmosphere. Nat. Commun. 11 (1), 1709. https://doi.org/10.1038/s41467-020-15495-3.
Zhang, Y., Sun, J.-G., Chen, Y.-J., Zhao, K.-Q., Gu, A.L., 2013. Re-Os and U-Pb geochronology of porphyry Mo deposits in Central Jilin Province: Mo ore-forming stages in northeast China. Int. Geol. Rev. 55 (14), 1763–1785. https://doi.org/10.1080/00206814.2013.794915.
Zhang, Y., Sun, J.-G., Xing, S.-W., Zhao, K.-Q., Ma, Y.-B., 2015. Geochronology and metallogenesis of porphyry Mo deposits in east-central Jilin province, China: Constraints from molybdenite Re-Os isotope systematics. Ore Geol. Rev. 71, 363–372. https://doi.org/10.1016/j.oregeorev.2015.06.014.
Zhang, Y., Sun, J.G., Xing, S.W., Zhao, K.Q., Ma, Y.b., Zhang, Z.J., Wang, Y., 2016. Ore-forming granites from Jurassic porphyry Mo deposits, east-Central Jilin Province, China: geochemistry, geochronology, and petrogenesis. Int Geol Rev. 58 (9), 1158–1174. https://doi.org/10.1080/00206814.2016.1150213.
Zhou, L.-L., Zeng, Q.-D., Liu, J.-M., Friis, H., Zhang, Z.-L., Duan, X.-X., Lan, T.-G., 2014. Geochronology of magmatism and mineralization of the Daheishan giant porphyry molybdenum deposit, Jilin Province, Northeast China: constraints on ore genesis and implications for geodynamic setting. Int Geol Rev. 56 (8), 929–953. https://doi.org/10.1080/00206814.2014.900728.
Zhou, L.-L., Zeng, Q.-D., Liu, J.-M., Friis, H., Zhang, Z.-L., Duan, X.-X., Chu, S.-X., 2015. Ore genesis and fluid evolution of the Daheishan giant porphyry molybdenum deposit, NE China. J Asian Earth Sci. 97, 486–505. https://doi.org/10.1016/j.jseaes.2014.09.037.
Zhou, L., Zeng, Q., Liu, J., Zhang, Z., Duan, X., 2018. What triggers fertile porphyritic Mo magmas in subduction setting: A case study from the giant Daheishan Mo deposit, NE China. Litho. 316-317, 212–231. https://doi.org/10.1016/j.lithos.2018.07.017.